Biaxial strain effects on the structure and stability of self-interstitial clusters in silicon

Robert J. Bondi, Sangheon Lee, and Gyeong S. Hwang*
Department of Chemical Engineering, University of Texas, Austin, Texas 78712, USA
(Received 7 October 2008; published 12 March 2009)

Using first-principles density-functional theory calculations, we examine variations in the structure and stability of small self-interstitial clusters ($I_n, n \leq 10$) in crystalline silicon across a range of biaxial strain conditions ($-3\% \leq \varepsilon \leq 3\%$) on Si(100). Under the strain conditions considered, there is no significant deviation in the ground-state configuration of any cluster from the strain-free case. However, the relative stability of I_4 and I_8 is significantly increased under both compressive and tensile strain conditions, while other cluster sizes generally show less sensitivity to changes in strain. This suggests that I_4 and I_8 likely play an even larger role in the clustering/dissolution of interstitial defects in strained Si relative to strain-free Si. We find that the noteworthy strain dependence of I_4 and I_8 is attributed to the unique shape and symmetry of the I_4-like core which allows reorientation within the lattice that is dependent on the compressive/tensile nature of biaxial strain.

DOI: 10.1103/PhysRevB.79.104106 PACS number(s): 61.72.−y

I. INTRODUCTION

Strain engineering has received intense attention in the semiconductor industry in the past few years as a vehicle to extend silicon complementary metal-oxide-semiconductor (CMOS) transistor performance in modern high-performance electronics. Relative to other CMOS enhancement techniques, incorporation of process strain only adds a few percent to wafer cost since only a few extra steps are required and often existing steps can simply be modified by tuning the strain of deposited thin films.[1] As a result, the semiconductor industry essentially adopted process-induced strain starting with the 90 nm node as a cost-effective technique to help sustain expected performance improvement consistent with Moore's law.

Si self-interstitial defects created by ion implantation are a topic of recent interest because they are associated with transient-enhanced diffusion of dopants during postimplantation annealing and subsequent degradation of dopant profiles that are critical in the formation of ultrashallow junctions. It is believed that extended {311} defects evolve from smaller nanoscale clusters of interstitial atoms,[2,3] although the mechanism for this process is still unclear. Small interstitial clusters have also proven harder to study and characterize than extended defects because their small size exceeds the resolution capabilities of many experimental instruments. Recent literature shows promising work in the study of small interstitial clusters using deep-level transition spectroscopy (DLTS) and evaluation of photoluminescence (PL) spectra from ion-implanted Si substrates.[2,3] The large variety of relatively stable configurations possible as cluster sizes increase will surely impede the task of correlating theory and experiment. Kinetic Monte Carlo (KMC) simulations predict the Ostwald ripening of interstitial clusters[2] and additionally provide a valuable means to determine the most stable atomic configurations of these clusters. Numerous recent articles acknowledge the general trend that interstitial clusters become more stable as size increases.[2,4,5] We hope to contribute to this field by identifying general trends of interstitial cluster stability incorporating parameters of cluster size, atomic configuration, and cluster orientation in the presence of strain.

There are essentially two different ways to apply strain to the channel of a metal-oxide-semiconductor field-effect transistor (MOSFET): biaxial strain, which is sometimes called global or bulk strain because it is implemented at the substrate level, and uniaxial strain, which is sometimes referenced as local or process-induced strain in the literature.[6] Biaxial strain is often implemented by building the entire transistor in strained Si epitaxy over a thick SiGe layer such as the example shown in Fig. 1. Since the thick relaxed SiGe layer is ultimately built on a Si wafer, this SiGe foundation is sometimes called a virtual substrate.[7] This ideally results in uniform tensile strain throughout the plane wherein the MOSFET drive current travels. Uniaxial strain can be implemented at the device level either by selectively growing Si epitaxy only in the source/drain recesses to impose strain only along the transistor channel direction or by depositing a high-stress silicon nitride cap layer which mechanically couples the local strain in the film into the underlying transistor channel. Uniaxial strain is largely preferred for CMOS processes because of better manufacturability and better return in electrical performance characteristics.[1,8] Biaxially strained Si suffers from larger defect densities and performance loss under large vertical electric fields.[1] Nevertheless, biaxially strained Si retains applications in other niches that justify further investigation. Most devices containing Si/SiGe heterostructures contain heteroepitaxial layers which contain an amount of biaxial strain dictated by the value of x in the

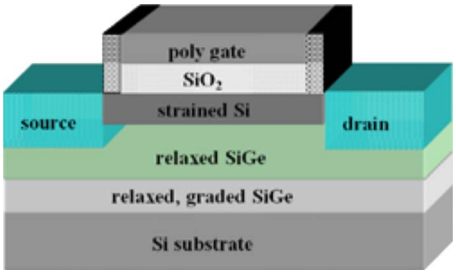

FIG. 1. (Color online) Cross section of a strained MOSFET device built on a SiGe virtual substrate.

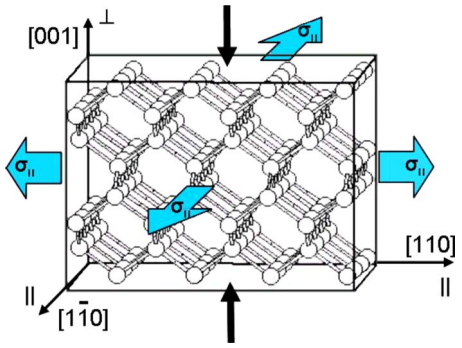

FIG. 2. (Color online) Tensile biaxial stress/strain interaction in our model Si supercell. In the figure, applied tensile stress, $\sigma_{\|}$, in the plane of the substrate acts equally in all directions as shown by block arrows and produces a tensile strain. In response, the lattice contracts in the out-of-plane direction as shown by the solid black arrows. Under compressive strain conditions, the directions of all arrows are inverted.

$Si_{1-x}Ge_x$ alloy. When a thin epilayer of Si is grown on a substantially thicker layer of $Si_{1-x}Ge_x$, biaxially strained Si results. Heterointerfaces of this nature can currently be found in modern heterojunction bipolar transistors (HBT) for high-speed and low noise applications, and Si/SiGe is also a viable material set for construction of modulation-doped field-effect transistors (MODFETs) in analog microwave applications requiring both low noise and high linearity.[7] In addition, another promising application for biaxially strained Si is in strained silicon on insulator (sSOI) which is an attractive material for fabricating fully depleted CMOS devices.[9]

In this paper, we will only examine the model case of small Si interstitial clusters in biaxially strained Si epitaxy grown on a relaxed SiGe (100) surface. Understanding this material system can reveal fundamental defect behaviors in the channel of advanced MOSFETs as shown by the device cross section in Fig. 1.[10,11] A (100) wafer surface is employed in our study since most CMOS devices are built on this particular substrate orientation. For the remainder of this article, "strain" will refer to biaxial strain on a Si (100) surface unless noted otherwise.

II. THEORETICAL BACKGROUND AND METHODS

In epitaxial growth, biaxial strain occurs in an epilayer when lattice mismatch is present between the epilayer and the substrate. If the lattice constant of the epilayer, a, is smaller than the lattice constant of the substrate, a_0, then tensile biaxial strain results. Conversely, if a is larger than a_0, compressive biaxial strain results. It is useful to define the lattice constant in the plane of strain as $a_{\|}$ and the lattice constant perpendicular to the plane of strain as $a_{\perp}$. In the regime of linear elastic behavior we model for Si, when $a_{\|}$ expands under tensile strain, $a_{\perp}$ simultaneously contracts. Under compressive strain, $a_{\|}$ contracts while $a_{\perp}$ expands. This phenomenon is known as the Poisson effect, as visualized in Fig. 2.[12]

We can quantify the Poisson effect for biaxially strained systems by defining a quantity, ν^*, that relates the ratio of in-plane strain, $\varepsilon_{\|}$, and out-of-plane strain, $\varepsilon_{\perp}$. In our system, the values of $a_{\|}$ in Si under tensile strain conditions are equal to representative values of a_{SiGe}, which is the lattice constant of a binary SiGe system. We calculate the in-plane strain as $\varepsilon_{\|}=(a_{SiGe}-a_{Si})/a_{Si}$ and the out-of-plane strain as $\varepsilon_{\perp}=(a_{\perp}-a_{Si})/a_{Si}$. The experimental value of a_{Si} is 5.4309 Å and a_{Ge} is 5.6461 Å,[13] so 4% tensile strain is the limiting case of Si grown over pure Ge. From linear elastic theory,[10,12–14] the relationship between out-of-plane and in-plane strain for a cubic crystal can be expressed in terms of two elastic stiffness constants,

$$\nu^* = -\varepsilon_{\perp}/\varepsilon_{\|} = 2(C_{12}/C_{11}). \quad (1)$$

Quantity ν^* is valid for deformations of a few percent strain. Using the values of 16.6×10^{11} and 6.4×10^{11} dyn/cm^2 for C_{11} and C_{12},[15] respectively, the value of ν^* is 0.771. Using ν^* and the expressions for $\varepsilon_{\|}$ and $\varepsilon_{\perp}$, we calculated the values of $a_{\perp}$ for each independent value of $a_{\|}$ studied. All results we present here for biaxially strained Si are based on $\nu^*=0.771$. By iterating through a reasonable range of $a_{\perp}$ for each value of $a_{\|}$ studied, we numerically verified that minimum-energy supercell dimensions occur as ν^* converges to 0.771.

To examine how the presence of biaxial strain influences the stability of small interstitial clusters, we first looked at their ground-state configurations under the strain-free condition. As recently reported by Lee and Hwang,[16,17] compact geometries are favored when the cluster size is smaller than ten self-interstitials. In Fig. 3, the ground-state compact configurations of small interstitial clusters considered here $(I_n, n\leq10)$ are presented; their different perspective views can also be found in the work reported by Lee and Hwang.[16,17] The small interstitial clusters were embedded inside either 256 or 480 atom supercells, depending on their size. Care was taken to ensure that each supercell size was large enough to accommodate a given cluster with no significant interaction with its periodic images. The supercells employed have two independent {110} facets in plane relative to strain and one independent {100} facet that responds with out-of-plane strain deformation, as depicted in Fig. 2.

For biaxial strain, there are two significant orientations of interest for compact clusters. The core and strained nearest neighbors in the compact I_4 configuration are shown in Fig. 4.[18,19] Examination of the figure shows that the I_4 cluster contains three C_2 symmetry axes. When the I_4 cluster core is embedded in bulk Si, these three C_2 axes map onto the three equivalent ⟨100⟩ directions in the crystal. The I_4 core and neighbor atoms will experience out-of-plane strain along the C_2^1 axis (coincides with S_4 rotation-reflection axis) and in-plane strain along the C_2^2 and C_2^3 axes under biaxial strain conditions as portrayed in Fig. 2. Since biaxial conditions eliminate one degree of freedom in the system, two cluster orientations—rather than three—are potentially unique. We extended this orientation-dependent strain modeling to all of our initial cluster orientations (shown in Fig. 3) by casting alternative orientations (marked by *) by transforming the out-of-plane cluster alignment to in-plane alignment. With reference to the crystal, this transformation moves the out-of-plane alignment from the [001] direction to either the

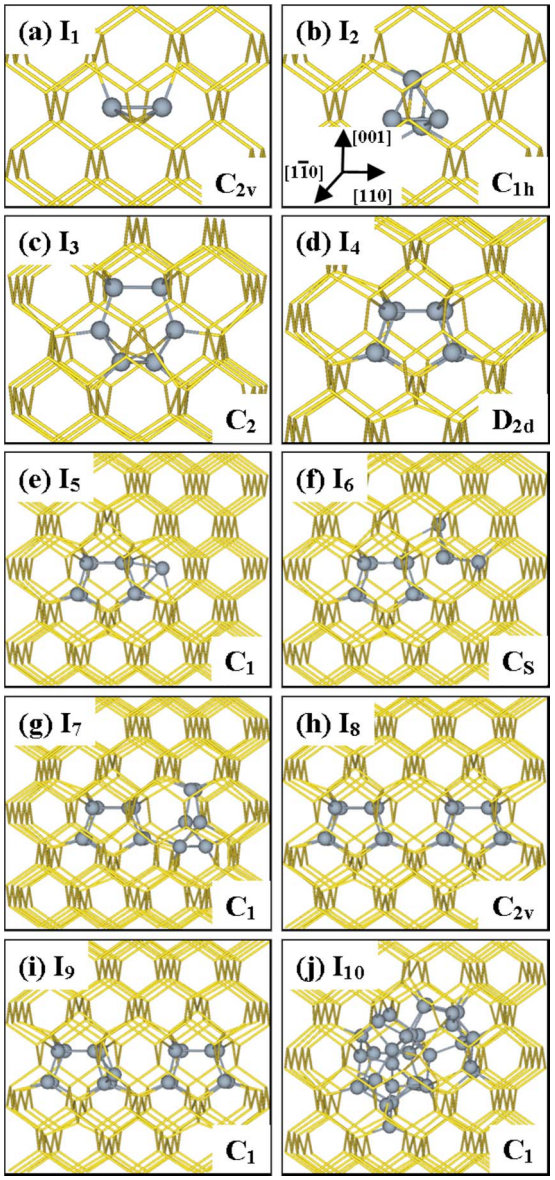

FIG. 3. (Color online) Ground-state configurations of small self-interstitial clusters $(I_n, n \leq 10)$ shown in their initial orientations with corresponding defect symmetries indicated. Light gray (gold) wireframe represents the bulk Si lattice. Dark gray spheres represent interstitial atoms and their highly strained neighbors.

[100] or [010] directions. For our model system, [100] and [010] are equivalent directions with respect to biaxial strain. These two orientations were evaluated at various strain conditions for possible minimum-energy configurations for all compact cluster sizes considered.[16] For completeness, we acknowledge that other orientations can be generated through pure rotation of the cluster applied to these two important orientations, but we observe the impact to strain-dependent cluster stability to be less significant.

All atomic structures and energies reported herein were calculated using a plane-wave basis set pseudopotential method within the generalized gradient approximation of Perdew and Wang (GGA-PW91) (Refs. 20 and 21) to density-functional theory (DFT),[22] as implemented in the

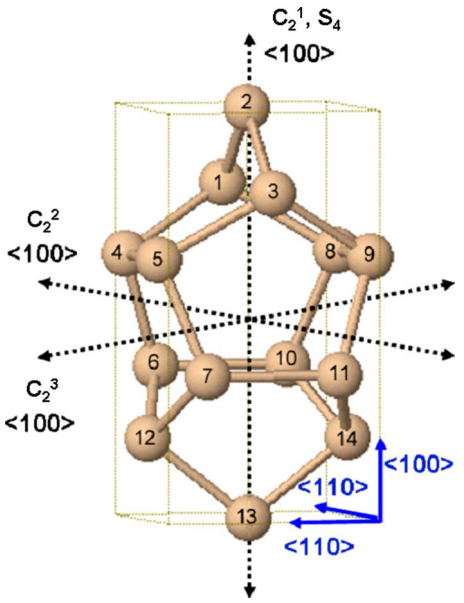

FIG. 4. (Color online) Cluster core and strained nearest neighbors that comprise the D_{2d} symmetry of the I_4 structure shown isolated from the Si lattice. The orientation shown is insensitive to strain. The three C_2 symmetry axes are shown in black. The S_4 rotation-reflection axis is coincident with the C_2^1 axis. Each C_2 axis is aligned with one of the ⟨100⟩ directions in the Si crystal. The blue axes along the bounding box provide reference to supercell orientation employed. The eight atoms at the center of the structure numbered 4 through 11 show interesting behavior as strain conditions vary. This central boat-shaped structure contains two pairs of bonds aligned along the ⟨110⟩ directions. These bond pairs are mutually orthogonal.

well-established Vienna *ab initio* simulation package (VASP).[23] Vanderbilt-type ultrasoft pseudopotentials[24] were used for core-electron interactions. Outer electron wave functions were expanded using a plane-wave basis set with a kinetic energy cutoff of 160 eV. The Brillouin zone sampling was performed with one k point (Γ) for geometric optimization. The geometric optimization allowed all atoms to relax until the total energy had converged within 1×10^{-3} eV tolerance. With the optimized ionic positions determined, corresponding total energies were re-evaluated using the $(2 \times 2 \times 2)$ Monkhorst-Pack grid. For the strain-free supercell, we used a fixed Si lattice constant of 5.457 Å along ⟨100⟩ or 3.859 Å along ⟨110⟩ as obtained from volume optimization. For each biaxial strain condition, we created a supercell with dimensions scaled using ν^*. A Perl script was generated to facilitate and manage running repeated VASP simulations across the range of strain conditions studied.

III. RESULTS AND DISCUSSION

Figure 5(a) presents a graphical trend of formation energy dependence on cluster size (n) for the selected conditions of −3%, 0%, and 3% uniform biaxial strain. The formation energy in terms of cluster size (n) and strain condition (ε), $E_f(n, \varepsilon)$, is given by

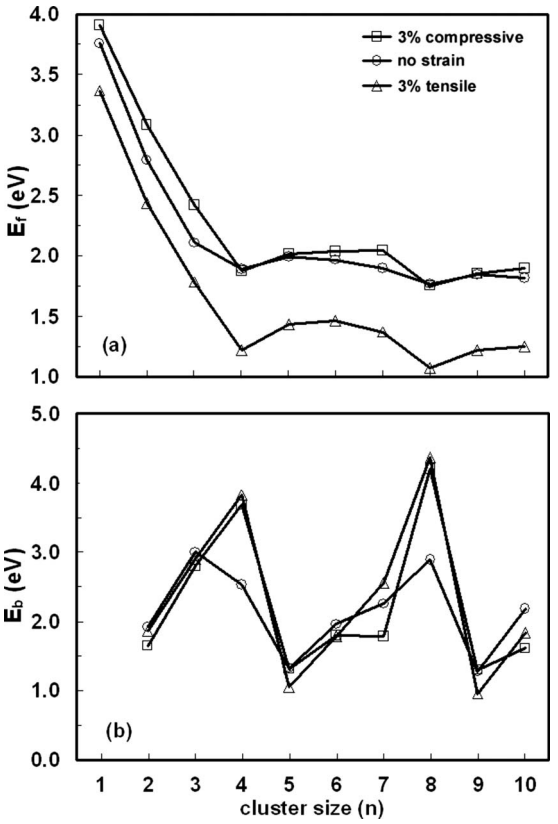

FIG. 5. (a) Formation energy and (b) binding energy dependencies as a function of cluster size for selected strain conditions as indicated. Each formation energy data point represents the most stable of multiple configuration and orientation combinations that were studied for each value of n. The binding energies are based on these same minimum formation energies and all reference the split-$\langle 110 \rangle$ I_1 configuration.

$$E_f(n,\varepsilon) = E_{\text{tot}}(n,\varepsilon) - \frac{n+N}{N} E_{\text{bulk}}(\varepsilon), \tag{2}$$

where $E_{\text{tot}}(n,\varepsilon)$ is the total energy of the I_n cluster in the $n+N$ atom supercell, n is the size of the interstitial cluster, N is the basis number of atoms in the bulk Si supercell, and $E_{\text{bulk}}(\varepsilon)$ is the total energy of the N atom supercell of crystalline Si at a given biaxial strain condition. Each data point represents the lowest formation energy per interstitial for a given strain condition among several configurations and orientations that we examined for a given cluster size. The work of Lee and Hwang[16,17] can be referenced for detailed structural configurations for the small clusters examined here. Our results for the strain-free case are in good agreement with previous studies.[16,17,25–27] Some debate has existed over the minimum-energy configuration of I_3, but we contend that the fourfold-coordinated structure in Fig. 3(c) is the ground state. We found the strain-free E_f to be 2.12 eV for the ground state I_3 configuration shown in Fig. 3(c) and 2.34 eV for the I_3 compact configuration also included in our study. Under the range of strain conditions considered ($-3\% \leq \varepsilon \leq 3\%$), we find that there is no significant deviation in the ground state cluster configurations from the strain-free case for the small clusters studied ($I_n, n \leq 10$). Exceeding a magnitude of 3% strain appears to cause the atomic configuration and bond topology of certain clusters to change substantially, so review of those results will be reserved for future work.

The general behavior observed from the family of E_f curves [Fig. 5(a)] is for most cluster configurations to stabilize as strain shifts from compressive to tensile and increasing cluster size also generally lowers E_f per interstitial at a given strain condition. The strain response under 3% compressive conditions is nearly the same as the strain response in the strain-free case, but 3% tensile strain shows a strong stabilizing effect on clusters of all sizes. The response of stabilization with increasing tensile strain is largely monotonic for most configurations. For interstitials, the stabilizing influence of tensile strain can be rationalized as the crystal lattice fundamentally becoming more accommodating to extra atoms as interatomic distances increase. It is worth noting that the minimum-energy configurations for $n \geq 4$ typically contain the I_4 compact configuration.[16,17]

Beyond the general trend of decreasing E_f with increasing cluster size, the local minima at $n=4$ and $n=8$ are also interesting. For the strain-free condition, this trend has also been described in previous studies[17] and is consistent with inverse model studies based on experimental findings.[4,5] Other results in the literature report oscillating behavior in the stability of small interstitial clusters using a variety of computational methods.[28,29] Ortiz *et al.*[4] justified the oscillating behavior in the stability of compact interstitial clusters by claiming that the capture of an extra interstitial by certain cluster sizes can considerably modulate the local stress the cluster imparts on the surrounding lattice. Subsequent lattice relaxation could then lead to a reduction in the system energy. Our results show that the formation energy minima at both $n=4$ and $n=8$ persist under both compressive and tensile strain conditions. From Fig. 5(a), it is also shown that strain of either sign deepens the minima at $n=4$ and $n=8$ relative to the E_f of the adjacent cluster sizes.

Annealing of interstitial defects may be preceded by dissociation into smaller clusters. Thus, we also calculate how the cluster binding energies, E_b, vary with cluster size and strain conditions. The results are summarized in Fig. 5(b). Here, the binding energy, which represents an energy cost for single interstitial liberation from a given cluster, is given by

$$E_b(n,\varepsilon) = (n-1)E_f(n-1,\varepsilon) + E_f(1,\varepsilon) - nE_f(n,\varepsilon), \tag{3}$$

where all formation energies are in units of eV/atom and reference the minimum-energy split-$\langle 110 \rangle$ configuration of a single interstitial, $E_f(1,\varepsilon)$. The reference $E_f(1,\varepsilon)$ values are computed to be 3.91, 3.76, and 3.37 eV under 3% compressive, strain-free, and 3% tensile strain conditions, respectively. The relative stability of I_4 and I_8 is emphasized by local peaks in binding energy. Similar to the E_f results, the presence of biaxial strain magnifies the peak binding energy at $n=4$ and $n=8$. While the I_4 binding energy is 2.53 eV in the strain-free case, it increases to 3.83 eV under 3% tensile strain and 3.68 eV under 3% compressive strain. Likewise, the I_8 binding energy increases from 2.90 eV in the strain-free case to 4.37 and 4.21 eV under 3% tensile and 3% compressive strain conditions, respectively. The low binding

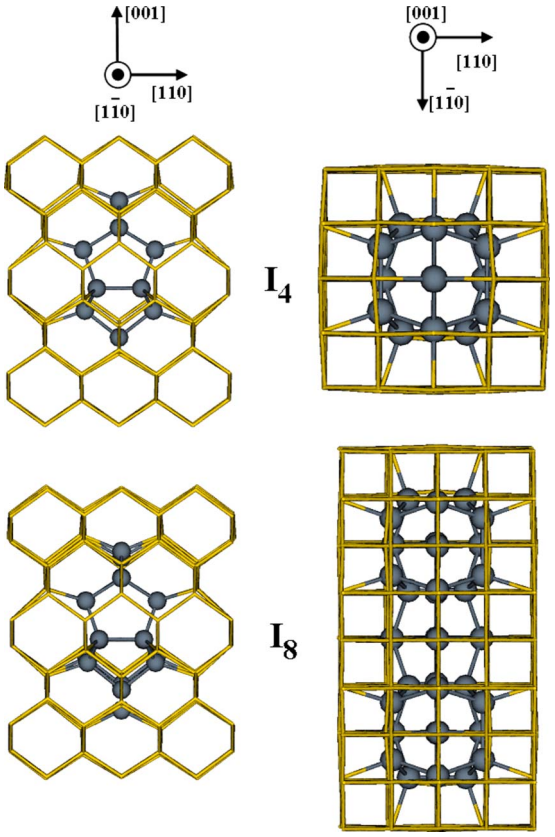

FIG. 6. (Color online) I_4 and I_8 clusters from two different perspectives embedded inside interior subsections of respective supercells. Light gray (gold) wireframe represents bulk Si atoms in the lattice. Dark gray spheres represent the interstitial atoms and their highly strained neighbors.

energies of I_5 and I_9 indicate that a single interstitial added to I_4 or I_8, respectively, is not tightly bound to the cluster. Our results suggest that I_4 and I_8 likely play an even larger role in the clustering/dissolution of interstitial defects in strained Si, compared to unstrained Si, because of their increased relative stability over other small compact clusters.

The important configurations of the I_4 and I_8 clusters are shown in detail from two different perspectives in Fig. 6. A high-symmetry perspective is seen along the [001] direction for both clusters. The relative orientation between the two constituent I_4 cores of I_8 within the Si lattice and subsequent effect on the interfacial bond topology was seen to have a non-negligible effect on the formation energy.[16,17] Figure 7 shows how E_f varies with biaxial strain for both I_4 and I_8 which highlights the significant impact that cluster orientation within the supercell can produce on cluster formation energy. In contrast, we also include the same plots for I_2 and I_3 to demonstrate that most clusters, in general, do not exhibit strong orientation-dependent formation energies under strained conditions. I_2 shows no orientation-dependent E_f response, while I_3 shows a weak response. We found that different cluster orientations often shift the qualification of adequate supercell size to avoid periodic image effects. To avoid excessively large supercell sizes, we equated the formation energies for all orientations at the strain-free condition to reference the lowest strain-free E_f found. This same E_f reference shift was then applied to all strain conditions. The inset graphics in all cases show the orientation of the clusters as viewed from out of plane with respect to strain. For the I_4 and I_8 structures, the S_4 rotation-reflection axis of the individual I_4 core is shown perpendicular to the plane of strain in the original orientation. In both cases, this represents the highest-symmetry perspective of the respective clusters.

The I_4 original orientation shows nearly invariant response to strain in Fig. 7(c) since E_f only varies by 0.01 eV from 3% compressive to 3% tensile strain; however, the alternative orientation, I_4^*, is 1.33 eV more stable at 3% tensile strain than at 3% compressive strain. It is instructive to refer to Eq. (2) and note that the invariant E_f response of the I_4 orientation to strain indicates that the total-energy change in the cluster must be nearly identical to the total-energy change in crystalline Si in response to strain. The I_8 cluster exhibits a dual-response strain behavior that is nearly identical to that of I_4. For other cluster configurations with less symmetry [such as I_2 and I_3 as seen in Fig. 7(a) and 7(b)], the equivalent orientation pair of E_f versus strain curves shows essentially degenerate or weaker orientation dependence.

Our calculations demonstrate that the particular shape of I_4 with D_{2d} symmetry contributes to its unique behavior. The I_4 core structure was previously introduced in Sec. II along with the argument for two relevant orientations in a biaxially strained system. Since each C_2 axis is aligned in an equivalent ⟨100⟩ direction in the diamond lattice of Si, it is possible for either orientation to prevail in the same wafer crystal orientation. The sign of strain should determine the prevailing orientation of I_4 compact.

The I_3 compact configuration with D_{2d} symmetry is compared to I_4 in Fig. 8 to demonstrate that the Shoenflies nomenclature[30] for point-group symmetry may not be sufficient to identify structures that will exhibit the dual-response strain behavior shown by I_4. Note that the I_3 compact configuration is not ground state but was included in our strain investigation. The I_3 compact configuration is essentially two split-⟨110⟩ interstitials in close proximity and orthogonal to each other with one atom from the lattice participating in the cluster. The I_3 compact configuration is approximately a perfect tetrahedron, but the angles subtended by the split-⟨110⟩ bonds are approximately 61°; therefore, all tetrahedron faces are isosceles triangles. As a result, we report the relaxed I_3 compact configuration to have D_{2d} symmetry, rather than the T_d symmetry exemplified by a methane molecule.[31] The I_3 compact configuration, like I_4, also has three C_2 axes, each aligned with one of the three ⟨100⟩ directions in Si. Figure 8 compares the shape and symmetry of I_3 compact and the I_4 structure along ⟨100⟩ directions. While both structures are classified with D_{2d} symmetry, the overall symmetry can be further resolved. While each structure has a C_2 symmetry axis aligned along one of the ⟨100⟩ crystal directions, only the I_3 compact configuration shows essentially the same atomic arrangement or cluster shape repeated through symmetry operations about all three C_2 axes. Note that the atomic arrangement along two of the three C_2 axes is slightly distorted from the atomic arrangement as viewed along the C_2 axis coincident with the S_4 rotation-reflection axis. This

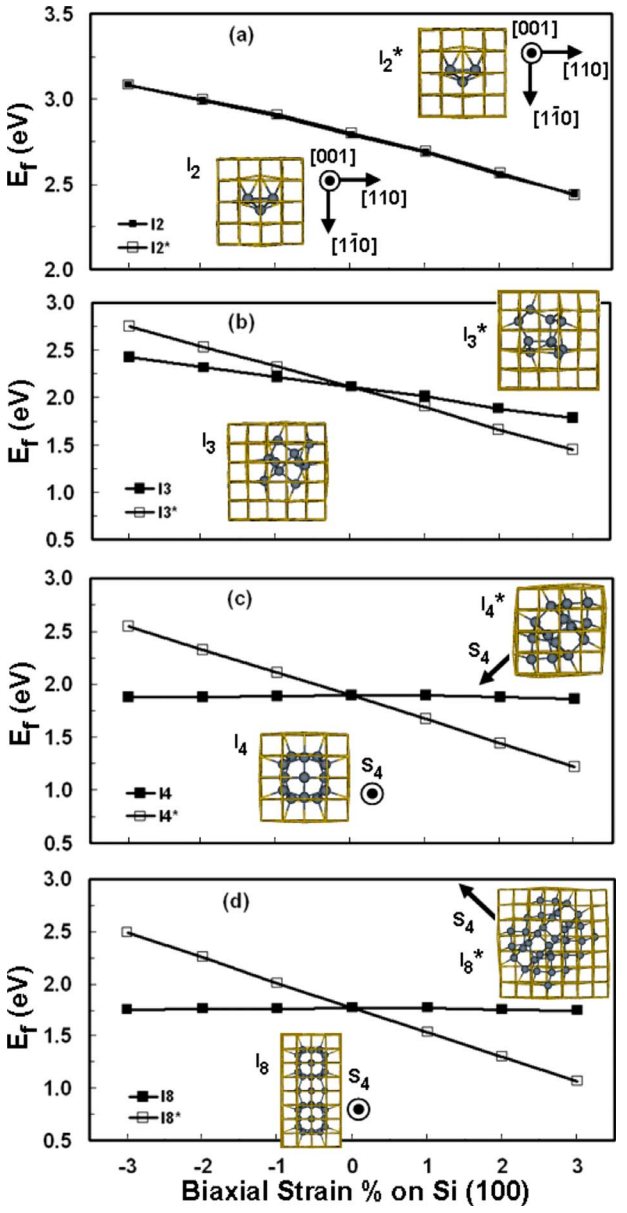

FIG. 7. (Color online) Formation energy response to biaxial strain compared and contrasted for different self-interstitial clusters as indicated. Inset graphics show how each structure is oriented within the supercell. Light gray (gold) wireframe represents the bulk Si lattice. Dark gray spheres denote the highly strained interstitial and neighboring atoms composing the core of the clusters. Plots (a) and (b) show weak to no difference in the strain response for the different orientations of the I_2 and I_3 clusters. In contrast, plots (c) and (d) quantify significantly different strain responses of different orientations of clusters bearing the compact I_4 core. Plot (c) shows the two relevant orientations of the I_4 configuration under biaxial strain, while plot (d) shows the same for the I_8 configuration. In both cases, the S_4 axis of a single I_4 core is shown to depict how each structure is transformed to make the alternative orientation. In both cases, when the S_4 axis is out of plane with respect to strain, the structure shows less sensitivity to biaxial strain. Orientations with this S_4 axis moved into the plane of strain are marked with a *. The presence of the I_4 core in both I_4 and I_8 configurations gives the two structures nearly identical strain responses with respect to orientation.

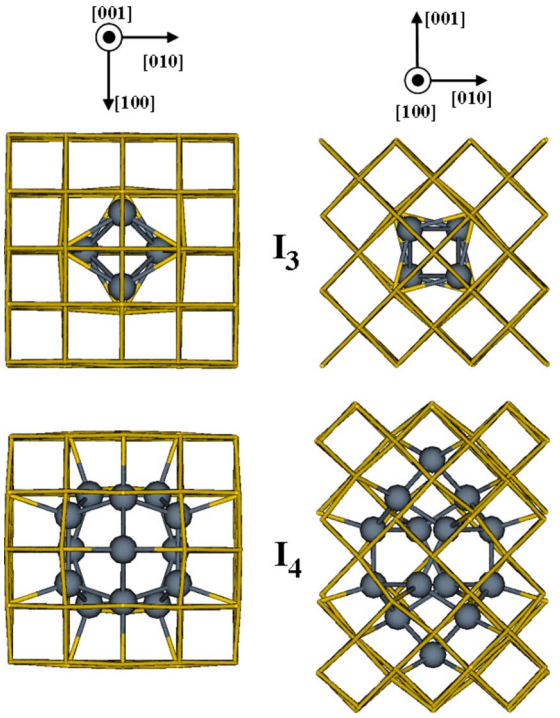

FIG. 8. (Color online) Comparison of the D_{2d} symmetry and shape of the I_3 compact and I_4 cluster configurations. The left and right perspectives show the configurations embedded in a subsection of the lattice as viewed along [001] and [100], respectively. For both clusters, the view along [010] (omitted) is identical to the view along [100]. Light gray (gold) wireframe represents the bulk Si lattice. Dark gray spheres represent interstitial atoms and their highly strained neighbors. Both structures have three C_2 axes and each is aligned along one of the ⟨100⟩ crystal directions. While both configurations are classified as D_{2d} symmetry, they are different. The configuration shape observed along the C_2 axes for I_3 compact is nearly identical along all ⟨100⟩ directions, while the configuration shape observed along the I_4 C_2 axis (coincident with S_4 axis) aligned with the [001] direction is clearly different than the configuration shape observed along the C_2 axes aligned with the [100] and [010] directions.

follows from the imperfect tetrahedral geometry. For the I_4 configuration, the atomic arrangement repeated through symmetry around the C_2 axis aligned with the [001] direction is different from the atomic arrangement transformed through symmetry around the C_2 axes aligned with the [100] and [010] directions. The shape and higher overall symmetry in I_3 compact make it appear approximately the same along the in-plane and out-of-plane directions; thus, the two relevant biaxial strain orientations produce similar strain responses. This suggests that the I_3 compact strain response is probably a consequence of the approximate T_d symmetry.

Further examination of the bond configuration in I_4 is useful to help elucidate some features that contribute to the dual-response strain effect. Figure 9 isolates the eight atoms from the boat-shaped core of the I_4 cluster (as shown in Fig. 4). There are two interesting bond pairs present (4–5, 8–9 and 6–10, 7–11), each of which is aligned along one of the ⟨110⟩ directions. Both of these bond pairs are in plane with respect to biaxial strain in the original orientation of I_4.

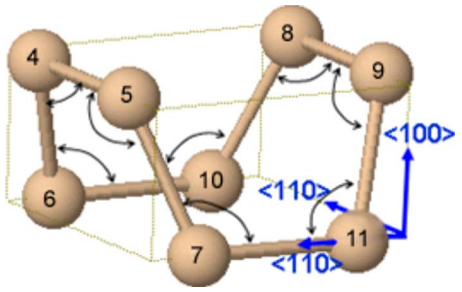

FIG. 9. (Color online) Boat-shaped central core of the I_4 cluster in the strain invariant orientation isolated from the larger structure in Fig. 4. The eight bond angles discussed in the text are shown in black.

When these bonds experience the full effect of biaxial strain, the strain response of I_4 is nearly invariant as previously discussed in reference to Fig. 7(c). In the alternative orientation of I_4 denoted as I_4^*, none of the core $\langle 110\rangle$-aligned bonds is fully within the plane of strain. Without these bonds experiencing and perhaps absorbing as much of the lattice strain deformation, the structure E_f is highly sensitive to changes in strain.

The bond lengths of the four $\langle 110\rangle$-aligned bonds in Fig. 9 were measured under all strain conditions studied for both orientations. In strain-free Si, the bond length of all four bonds is 2.34 Å in both orientations, which is slightly compressive relative to the equilibrium Si bond length of 2.36 Å. The response of the bond lengths to strain was similar for both I_4 and I_4^*. Compressive strain reduces all four bond lengths uniformly, while tensile strain stretches all four bond lengths uniformly.

The response of the bond angles in the boat-shaped core to biaxial strain is more interesting. Table I summarizes the average and standard deviation of the eight bond angles in the boat-shaped core of I_4 across all strain conditions evaluated for both cluster orientations. Under strain-free conditions, the average bond angle is about 108.0°, which is slightly smaller than the 109.5° angle found in perfect, crystalline Si. The bond angle response to strain is opposite between the two orientations. The average bond angle increases with increasingly tensile strain for I_4 but decreases with increasingly tensile strain for I_4^*. At any strain condition, the lowest E_f corresponds to the orientation with the lowest average bond angle in the boat-shaped core.

TABLE I. Average ($\bar{x}_{ba}$) and standard deviation (σ_{ba}) of the eight bond angles in the boat-shaped core of the I_4 cluster for all biaxial strain conditions evaluated for both cluster orientations. All bond angle statistics are presented in units of degrees.

	I_4		I_4^*	
Strain %	$\bar{x}_{ba}$	σ_{ba}	$\bar{x}_{ba}$	σ_{ba}
−3	106.9	0.00	108.7	1.38
−2	107.3	0.05	108.4	1.13
−1	107.6	0.05	108.2	0.85
0	108.1	0.00	108.0	0.55
1	108.5	0.04	107.8	0.34
2	108.8	0.07	107.7	0.29
3	109.1	0.07	107.5	0.40

The bond angle distributions also help distinguish the two orientations under strain. Among the eight bond angles of concern as shown in Fig. 9, the I_4 orientation bond angles all change uniformly under strain so the standard deviation, σ_{ba}, of bond angles is small and all bond angles are virtually identical. For I_4, $\sigma_{ba} < 0.1°$ for all strain conditions studied. In contrast, the I_4^* orientation does not compress/stretch as uniformly under strain because σ_{ba} is much larger for all strain conditions. Under increasingly compressive strain conditions, σ_{ba} correspondingly increases to its highest value of 1.38° under 3% compressive strain for I_4^*. Increasing compressive strain increases the bond angle deviations from 108.0°, which consequently increases the strain energy. The increased strain energy explains why the I_4^* E_f increases rapidly as conditions become more compressive. The deviation in bond angle shows symmetry about the average for I_4^*. Each bond angle larger than the average is paired with a corresponding bond angle that is smaller than the average by the same amount. Visually, this corresponds to the boat-shaped core of I_4^* folding as strain is applied.

IV. CONCLUSIONS

The effect of uniform biaxial strain on the structure and stability of small self-interstitial clusters $(I_n, n \leq 10)$ in Si was investigated using first-principles density-functional theory calculations. For the strain range of $-3\% \leq \varepsilon \leq 3\%$, our work reveals an interesting cluster stability dependence on the relative orientation between the interstitial cluster and the strained bulk Si lattice, while we see no significant deviation in the ground-state cluster configuration from the strain-free case. The observation of orientation-dependent strain response strongly correlates to the presence of the I_4 cluster core for cluster sizes of $n \geq 4$ interstitials. This orientation dependence and sign of applied biaxial strain can influence the prevailing orientation of clusters in strained systems and may even prove to dictate the minimum-energy cluster configuration. The unique strain response of the I_4 core allows it to adapt to different strain conditions through reorientation. As a result, minimum-energy configurations for compact clusters with $n > 4$ often contain the I_4 core structure. We also find that either inadequate or excessive cluster symmetry can destroy the unique dual-response strain behavior observed for the I_4 compact cluster configuration. Structures with the most symmetry have a higher probability of producing an identical strain response when reoriented. Like I_2, small clusters with little symmetry tend to produce more of an isotropic response, so reorientation of the cluster has a weak effect, if any, on the strain response. Our study also shows that the unique strain response of the I_4 cluster is not only driven by the cluster symmetry but also the interaction of the cluster symmetry with the geometry of the diamond lattice of Si and the response of this lattice orientation to biaxial strain.

ACKNOWLEDGMENTS

We acknowledge Semiconductor Research Corporation (Contract No. 1413-001), National Science Foundation (Contract No. CAREER-CTS-0449373), and Robert A. Welch Foundation (Contract No. F-1535) for their financial support. We would also like to thank the Texas Advanced Computing Center for use of their computing resources.

*Author to whom correspondence should be addressed: gshwang@che.utexas.edu

[1] S. E. Thompson, Guangyu Sun, Youn Sung Choi, and Toshikazu Nishida, IEEE Trans. Electron Devices **53**, 1010 (2006).
[2] J. Kim, F. Kirchhoff, J. W. Wilkins, and F. S. Khan, Phys. Rev. Lett. **84**, 503 (2000).
[3] P. K. Giri, Semicond. Sci. Technol. **20**, 638 (2005).
[4] C. J. Ortiz, P. Pichler, T. Fuhner, F. Cristiano, B. Colombeau, N. E. B. Cowern, and A. Claverie, J. Appl. Phys. **96**, 4866 (2004).
[5] N. E. B. Cowern, G. Mannino, P. A. Stolk, F. Roozeboom, H. G. A. Huizing, J. G. M. van Berkum, F. Cristiano, A. Claverie, and M. Jaraiz, Phys. Rev. Lett. **82**, 4460 (1999).
[6] K. Derbyshire, Solid State Technol. **50**, 38 (2007).
[7] D. J. Paul, Semicond. Sci. Technol. **19**, R75 (2004).
[8] K.-J. Chui, K.-W. Ang, N. Balasubramanian, M.-F. Li, G. S. Samudra, and Y.-C. Yeo, IEEE Trans. Electron Devices **54**, 249 (2007).
[9] R. Harper, Mater. Sci. Eng., B **134**, 154 (2006).
[10] L. Lin, T. Kirichenko, B. R. Sahu, G. S. Hwang, and S. K. Banerjee, Phys. Rev. B **72**, 205206 (2005).
[11] J. L. Hoyt, H. M. Nayfeh, S. Eguchi, I. Aberg, G. Xia, T. Drake, E. A. Fitzgerald, and D. A. Antoniadis, in *IEEE International Electron Devices Meeting*, San Francisco, 2002 (IEEE, 2002), pp. 23–26.
[12] P. Bhattacharya, *Semiconductor Optoelectronic Devices* (Prentice Hall, Upper Saddle River, NJ, 1997).
[13] J. Singh, *Physics of Semiconductors and Their Heterostructures* (McGraw-Hill, New York, 1993).
[14] C. G. Van de Walle and R. M. Martin, Phys. Rev. B **34**, 5621 (1986).
[15] M. E. Levinshtein, S. L. Rumyantsev, and M. S. Shur, *Handbook Series on Semiconductor Parameters* (World Scientific, London, 1996), Vol. 1, p. 29.
[16] S. Lee and G. S. Hwang, Phys. Rev. B **77**, 085210 (2008).
[17] S. Lee and G. S. Hwang, Phys. Rev. B **78**, 045204 (2008).
[18] N. Arai, S. Takeda, and M. Kohyama, Phys. Rev. Lett. **78**, 4265 (1997).
[19] B. J. Coomer, J. P. Goss, R. Jones, S. Oberg, and P. R. Briddon, J. Phys.: Condens. Matter **13**, L1 (2001).
[20] J. P. Perdew, K. Burke, and M. Ernzerhof, Phys. Rev. Lett. **77**, 3865 (1996).
[21] J. P. Perdew and Y. Wang, Phys. Rev. B **45**, 13244 (1992).
[22] G. Kresse and J. Hafner, Phys. Rev. B **47**, 558 (1993); **49**, 14251 (1994); G. Kresse and J. Furthmuller, Comput. Mater. Sci. **6**, 15 (1996); Phys. Rev. B **54**, 11169 (1996).
[23] G. Kresse and J. Furthmuller, *VASP the Guide* (Vienna University of Technology, Vienna, 2001).
[24] D. Vanderbilt, Phys. Rev. B **41**, 7892 (1990).
[25] G. M. Lopez and V. Fiorentini, Phys. Rev. B **69**, 155206 (2004).
[26] D. A. Richie, J. Kim, S. A. Barr, K. R. A. Hazzard, R. Hennig, and J. W. Wilkins, Phys. Rev. Lett. **92**, 045501 (2004).
[27] W.-K. Leung, R. J. Needs, G. Rajagopal, S. Itoh, and S. Ihara, Phys. Rev. Lett. **83**, 2351 (1999).
[28] L. Colombo, Physica B **273-274**, 458 (1999).
[29] M. Gharaibeh, S. K. Estreicher, and P. A. Fedders, Physica B **273-274**, 532 (1999).
[30] N. W. Ashcroft and N. D. Mermin, *Solid State Physics* (Thomson Learning, U.S.A., 1976).
[31] T. Engel and P. Reid, *Physical Chemistry* (Pearson Education, Inc., New York, 2006).